

## Chapter 3

# Modeling of PV-WECS Based Microgrid

### Introduction

The power generation in the MG is mainly based on the renewable energy sources (RES). They are becoming increasingly attractive to consumers as a great number of them are installed at consumer's sites. In the present work two RESs, PV and Wind are considered to constitute the MG. The generating units based on these RES's are modeled to form the MG and supply of quality power to the local load is studied. RES based power generation is not a constant source of the supply as the power generated directly relies on the environmental conditions. The challenge is maintaining the output voltage at constant. In addition, linear and nonlinear loads connected to the MG also affect the power quality in the MG. The power quality issues occurring during load and generation balance in MG is examined in this chapter.

### 3.1 Modeling of Microgrid

A microgrid is a power supply network in which a cluster of small on-site generators provide power for a small community such as homes, parks, and office buildings. The increasing interest

in a microgrid is changing the dependency on the conventional centralized power system. In this conventional system, power is generated mainly by combustion of fossil fuels (coal, oil, and gas), nuclear and hydropower where the power is delivered over long distances to consumers [3]. In the centralized power system, power transmission from a large source to several utilities can create shortcomings in the efficient power supply. Conversely, microgrid technology is an alternative technique for the requirement of the future power system. The key advantages are a better quality of the service, increased efficiency, and specific economic interests. The power generation in MG is mainly based on RESs. The surplus power from the MG can be exchanged with the utility grid [4]. The two different operating modes of microgrid are grid interconnected and islanded modes (which is also referred to as stand-alone). Major elements of MG are shown in the block diagram given in Figure. 1.1. An MG constituting of two DGs based on wind and solar energy is formed. PV generation consists of PV panels connected in series forming a string, and such strings are connected in parallel to form an array to achieve the desired output power from PV generation. The output voltage from the PV is stepped up to the desired DC level using boost converter as shown in Figure. 3.1. The wind generation consists of wind turbine

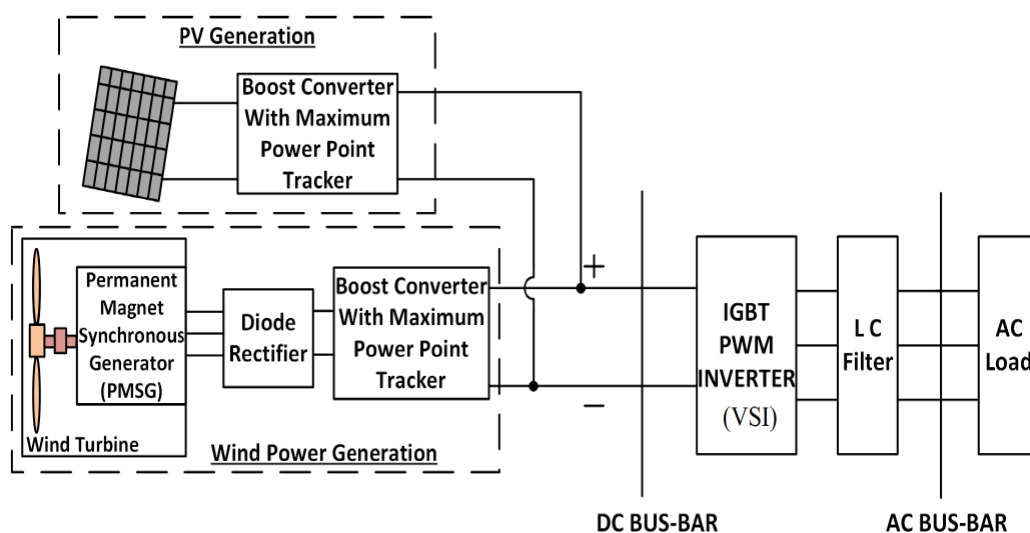


FIGURE 3.1: Schematic diagram of PV-WECS MG

coupled to Permanent Magnet Synchronous Generator (PMSG) whose output voltage is rectified using diode bridge rectifier and stepped up to the desired DC level using boost converter. The combined DC output of the MG is converted to AC using a voltage source inverter (VSI). Any

harmonics in the DC to AC conversion are minimized using LC filter [119]. This MG can be operated in stand-alone or grid integrated mode. An accurate model is required for analyzing the performance of PV based generation and wind energy conversion system (WECS) under different varying conditions. The following sections discuss the modeling and analysis of PV based generation and WECS generation in detail.

## 3.2 PV Based Generation

### 3.2.1 Selection of PV Model

The power from the PV panels is dependent on the solar illumination and operating temperature. Before selecting a PV panel it is essential to analyze the performance of PV panel under varying operating temperature from 25° C to 50°C and solar irradiation from 1000 W/m<sup>2</sup> to 200 W/m<sup>2</sup> [120]. The performance can be analyzed with a detailed mathematical model of PV module. Thus modeling of PV cell is vital [121].

The mathematical model is simulated to bring out the Power (P)-Voltage (V) and Current (I)-Voltage (V) characteristics under standard and non-uniform conditions. However, estimating the performance of the PV panel model in the real environment compared to manufacturer's data-sheet is a challenge. The reason being the electrical parameters of PV panel is computed under standard test conditions (STC) i.e. 25° C and 1000 W/m<sup>2</sup> from the manufacturer [122]. The simulated characteristics of the PV cell models are compared with the manufacturer's data-sheet curves in order to validate the simulated results. Modeling of diode-based PV cell could be developed depending upon the parameters involved in the design as shown in Table 3.1. They can be of from 3, 4 or 5 elements with 4, 5 or 8 parameters respectively involving single or two diodes including series and shunt resistance. The elements and parameters involved in the design of a PV cell are also listed in Table 3.1. Studies are conducted under different solar irradiance levels and effect of a change in series resistance is observed [123–125]. The effect of shunt resistance in the equivalent circuit of single diode PV model with 5 parameters is investigated under different solar irradiation levels [126–128]. Mathematical modeling of diode-based PV cell is developed

TABLE 3.1: The elements and parameters involved in the design of a PV cell

3-element or 4-parameter		4-element or 5-parameter		5-element or 8-parameter	
Element	Parameter	Element	Parameter	Element	Parameter
Current Source	$I_{PH}$	Current Source	$I_{PH}$	Current Source	$I_{PH}$
Diode	$I_D$	Diode	$I_D$	Diode	$I_D$
Output current (I)		Output current (I)		Output current (I)	
Series Resistance	$R_s$	Series Resistance	$R_s$	Series Resistance	$R_s$
		Shunt Resistance	$R_p$	Shunt Resistance	$R_p$

TABLE 3.2: Electrical parameters of manufacturer data sheet

Open Circuit Voltage	0.665 V
Short Circuit Current	5.75 A
Rated Power	3.0 W
Maximum Power Voltage	0.560 V
Maximum Power Current	5.35 A
Efficiency	20 % minimum
Temperature Co-efficients	
Voltage	-1.9 mV/ °C
Power	-0.38 % / °C

for all the above three different configurations with equation-based models of PV cell and are implemented in Simulink. Each PV cell is modeled to generate open circuit voltage of 0.665 V, short circuit current of 5.75 A and rated power output of 3 W. The results are compared under STC and validated by comparing with the referenced manufacturer's data sheet as shown in Table 3.2 [129].

### 3.2.1.1 Reference SUNPOWER A-300 Solar Cell, Mono Crystalline Silicon Datasheet

The I-V characteristic of the reference solar cell from the data-sheet is shown in Figure 3.2. The electrical parameters of the reference PV cell are shown in Table 3.2 [129]. These values from Table. 3.2 are substituted in the simulation models and simulated in order to obtain the characteristics similar to that shown in Figure 3.2. In the following section, a validation study is done by comparing the obtained simulated results with the Sun power A-300 solar cell characteristics and electrical parameters from the manufacturer's data sheet.



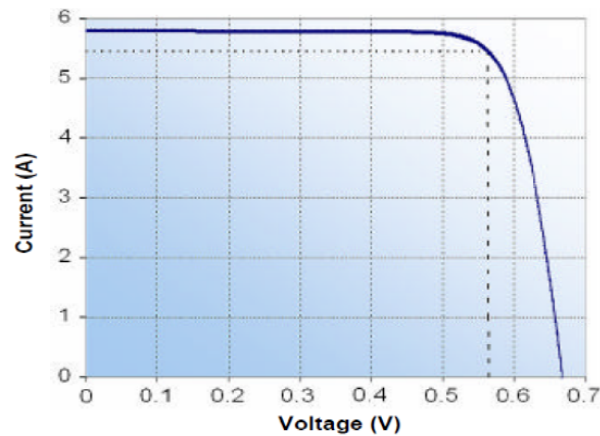


FIGURE 3.2: I-V Characteristics from Data-sheet.

### 3.2.1.2 Comparison of PV cell Models with PV Cell Model from Manufacturer Datasheet:

The different configurations analyzed for a PV cell model mentioned in [130] are

1. **Model-A:** O/C Voltage and S/C current, 5 parameters single diode
2. **Model-B:** By Equivalent circuit parameters, 5 parameters single diode
3. **Model-C:** By Equivalent circuit parameters, 8 parameters two diode

The P-V and I-V characteristics of the different PV cell models are simulated. The simulated characteristics are compared with the characteristics given in the manufacturer's data sheet [130]. The I-V characteristic extracted from manufacturer's datasheet plotted in Figure 3.2 is used for validation. Similarly, the simulated electrical parameters such as  $V_{OC}$ ,  $I_{SC}$ ,  $V_{mpp}$ ,  $I_{mpp}$  etc. of different PV cell models are compared with real-time values of electrical parameters extracted from the manufacturer's data sheet. A comparative analysis of electrical parameters of all the models of PV cell and manufacturer's data sheet are tabulated in Table 3.3. The comparative study is performed to select an accurate mathematical model of PV cell. The simulation study is conducted under STC. It is stated in [130] that the model "Equivalent circuit, 8 parameters two diode" of PV cell is implemented by equation based implementation i.e. Models 'C' produces the

TABLE 3.3: Simulation results of PV models in MATLAB/Simulink

Characteristics	Data-sheet	Simulink Model		
	SUN POWER A-300	Model-A	Model-B	Model-C
$V_{OC}$ (V)	<b>0.665</b>	0.671	0.685	<b>0.665</b>
$I_{SC}$ (A)	<b>5.75</b>	5.7	5.752	<b>5.743</b>
$W_{mpp}$ (W)	<b>3.0</b>	<b>2.996</b>	2.753	<b>3.008</b>
$V_{mpp}$ (V)	<b>0.560</b>	<b>0.559</b>	0.554	<b>0.556</b>
$I_{mpp}$ (A)	<b>5.35</b>	<b>5.363</b>	5.061	<b>5.413</b>
Irradiance ( $W/m^2$ )	<b>1000</b>	1000	1000	<b>1000</b>
Temperature ( $^{\circ}C$ )	<b>25</b>	25	25	<b>25</b>

output characteristics similar to that of the data sheet [131]. Thereby this model is considered to be an accurate PV model for developing PV based generation in the microgrid [130].

### 3.2.2 Equation Based Two-Diode-8 Parameter PV cell Modeling

General mathematical models of PV cell were proposed by various researchers [124, 132–134]. A two-diode model of PV cell is selected whose equivalent circuit diagram is shown in Figure 3.3. The mathematical model of two-diode PV cell performance is better as compared with the numerous models of single-diode model of PV cell under low illumination levels [130, 134]. The two-diode PV cell shown in Figure 3.3 consists of photo-generated current ( $I_{PH}$ ), two diodes with diode currents ( $I_{D1}$ ,  $I_{D2}$ ), shunt current  $I_{SH}$ , series Resistance ( $R_s$ ), shunt Resistance ( $R_p$ ), output voltage (V) and PV current (I or  $I_{PV}$ ). The relation between the output current and voltage can be obtained by using Kirchoff's Current Law (KCL) as given by equation (3.1).

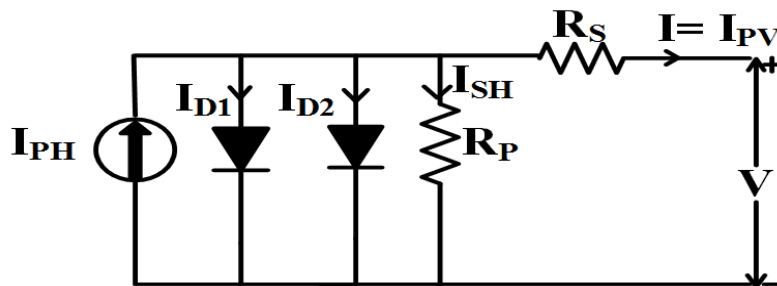


FIGURE 3.3: Equivalent circuit of a two diode PV model

$$I_{PV} = I_{PH} - I_{D1} - I_{D2} - I_{SH} \quad (3.1)$$

where,  $I_{D1}$ ,  $I_{D2}$  are the diode currents due to diffusion and are given by (3.2), (3.3).

$$I_{D1} = I_{s1} \left[ \exp \left( \frac{q \times V}{N_1 \times k \times T} \right) - 1 \right] \quad (3.2)$$

$$I_{D2} = I_{s2} \left[ \exp \left( \frac{q \times V}{N_2 \times k \times T} \right) - 1 \right] \quad (3.3)$$

where,  $I_{s1}$ ,  $I_{s2}$  are the reverse saturation currents of diode  $D_1$ ,  $D_2$ ,  $q$  is the charge on electron ( $1.602 \times 10^{-19}C$ ),  $V$  is the cell output voltage,  $N_1$ ,  $N_2$  are the quality factors of diode  $D_1$ ,  $D_2$ ,  $k$  is the Boltzmann constant ( $1.38 \times 10^{-23}$ ), and  $T$  is the junction temperature. The practical PV modules have the  $R_s$  and  $R_p$  as indicted in Figure 3.3. These parameters are incorporated to build the mathematical model of PV cell to replicate the practical PV cell. The equations (3.2), (3.3) can be modified as (3.4), (3.5).

$$I_{D1} = I_{s1} \left[ \exp \left( \frac{V + R_s \times I}{N_1 \times V_t} \right) - 1 \right] \quad (3.4)$$

$$I_{D2} = I_{s2} \left[ \exp \left( \frac{V + R_s \times I}{N_2 \times V_t} \right) - 1 \right] \quad (3.5)$$

where,  $V_t = \frac{N_s \times k \times T}{q}$  is the thermal voltage of the module with  $N_s$  being number of cells connected in series, the current in the shunt resistance is given by (8):

$$I_{SH} = \frac{V + R_s * I_{pv}}{R_p} \quad (3.6)$$

Substituting (3.4), (3.5), (3.6) in (3.1) we get the relation between the voltage and current of the two diode equivalent of the PV cell as (3.7).

$$I = I_{ph} - I_{s1} \left[ e^{\left( \frac{V + R_s \times I}{N_1 \times V_t} \right)} - 1 \right] - I_{s2} \left[ e^{\left( \frac{V + R_s \times I}{N_2 \times V_t} \right)} - 1 \right] - \frac{V + (R_s \times I_{pv})}{R_p} \quad (3.7)$$

The implementation of the two diode model of PV cell is shown in Figure 3.4. The block "TWO DIODE MODEL OF PV CELL" is a subsystem containing the equation based implementation of the PV cell (Eq. 3.7) which is shown in Figure 3.5. The values of  $R_s$  and  $R_p$  are calculated iteratively using the values  $V_{OC}$  and  $I_{SC}$ . The computed values of  $R_s$  and  $R_p$  are used to make

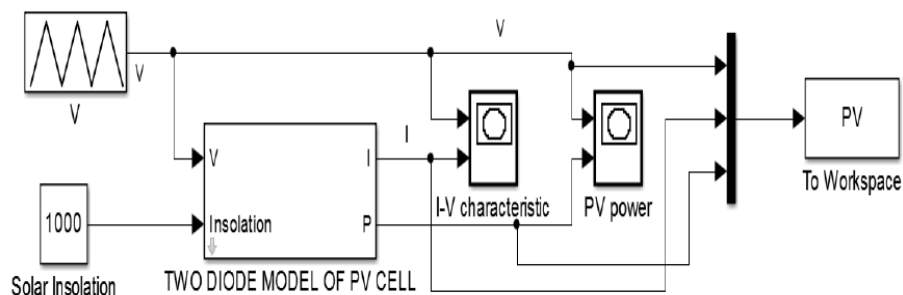


FIGURE 3.4: Simulink implementation of 2-diode PV cell model

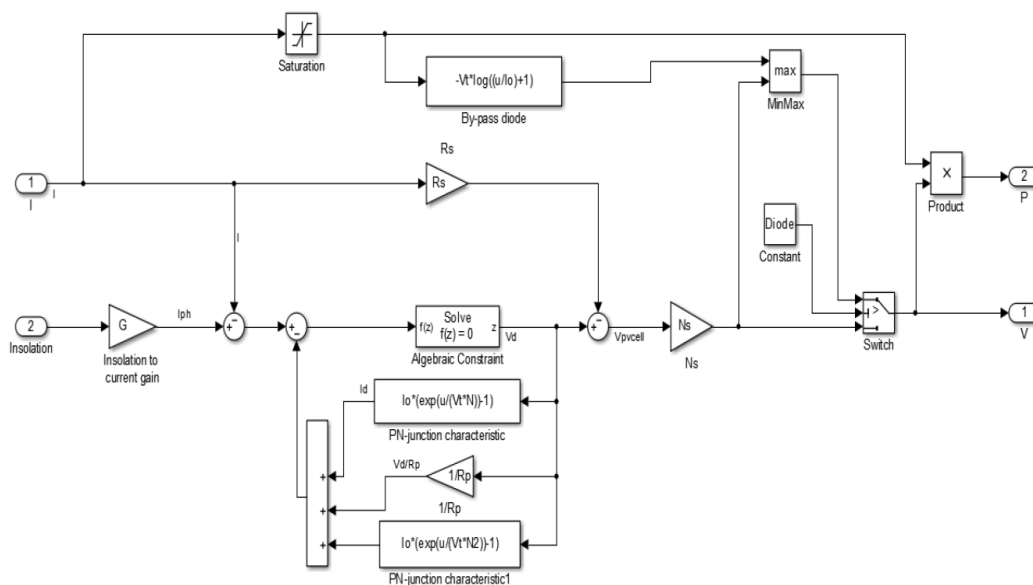


FIGURE 3.5: Simulink implementation of 2-diode PV cell model

the maximum point of the P-V curve simulated to coincide with the maximum point of the practical P-V curve of the PV module taken from data-sheet discussed in the following section.

### 3.2.2.1 Manufacture Datasheet of PV Panel

Sharp NU-E245 (J5) solar panel having P-V & I-V characteristics is shown in Figure. 3.6(a). The model consists of 50 cells of Silicon nitride multi-crystalline silicon cells to generate open circuit voltage of 37.5 V and Short circuit Current of 8.73 A with a power output of 245 W under  $1000 \text{ W} / \text{m}^2$  solar irradiation and at  $25^\circ \text{C}$  operating temperature. The electrical parameters of the SX 3200 are shown in Table. 3.4. Figure. 3.6(a) shows the I-V and P-V characteristics taken from the datasheet [149]. The equation based two-diode PV panel is modeled in Simulink. The corresponding I-V and P-V characteristics under different solar irradiation levels are obtained.

TABLE 3.4: Electrical parameters of SHARP NU-E245 (J5) from data sheet

Parameter	Notation	Value
Maximum Power	$P_{mpp}$	245 W
Open-Circuit Voltage	$V_{OC}$	37.5 V
Short-Circuit Current	$I_{SC}$	8.73 A
Voltage at Maximum Power Point	$V_{mpp}$	30.5 V
Current at Maximum Power Point	$I_{mpp}$	8.04 A
Efficiency	$\eta_m$	14.9
Nominal Operating Cell Temperature (NOCT)	-	47.5
Temp. Co-efficient Voltage	$\alpha V_{OC}$	-130
Temp. Co-efficient Current	$\alpha I_{SC}$	+0.053
Temp. Co-efficient Power	$\alpha P_{max}$	-0.485

These simulated I-V and P-V characteristics shown in Figure. 3.6(b) are compared with the characteristics of SHARP NU-E245 (J5) from data sheet shown in Figure. 3.6. Comparisons

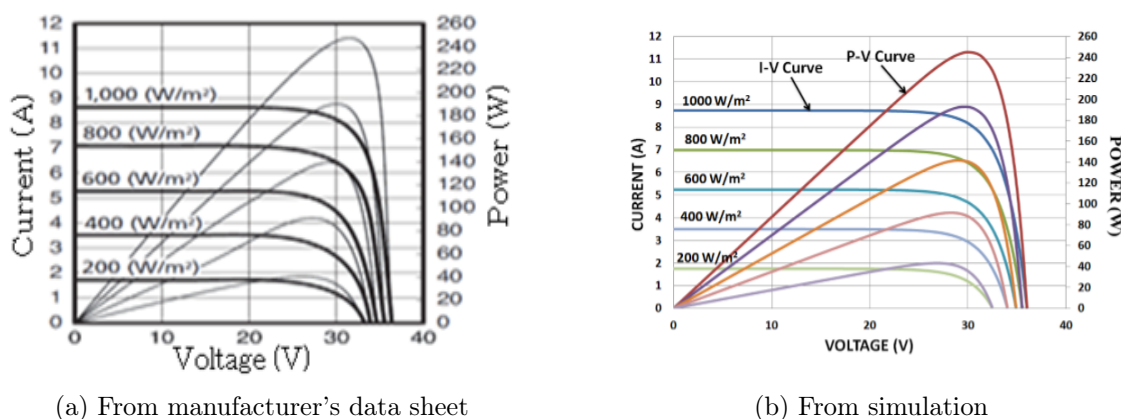


FIGURE 3.6: Comparison of I-V and P-V characteristics of manufacturer's data sheet and simulation

of the electrical parameters obtained at STC from simulation with the electrical parameters of the manufacturer data-sheet are tabulated in Table 3.5. It can be observed that both the

TABLE 3.5: Comparison of electrical parameters of manufacturer's data sheet and two diode model of PV cell

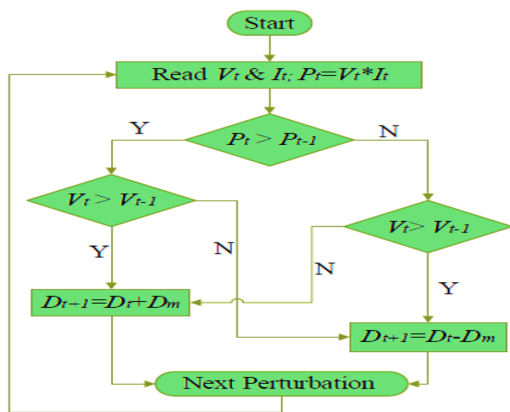
Electrical Parameters	Manufacturer Data-Sheet	Two-diode model of PV cell in Simulink
$V_{OC}$	37.5 V	37.5 V
$I_{SC}$	8.73 A	8.729 A
$P_{max}$	245 W	245 W
$V_{mpp}$	30.5 V	30.75 V
$I_{mpp}$	8.04 A	8.04 A

simulated electrical parameters of the PV panel fairly coincide with the manufacturer's data-sheet parameters. The output voltage of PV panel is stepped up to the desired level using a boost converter. Modeling of the boost converter is explained in the next section.

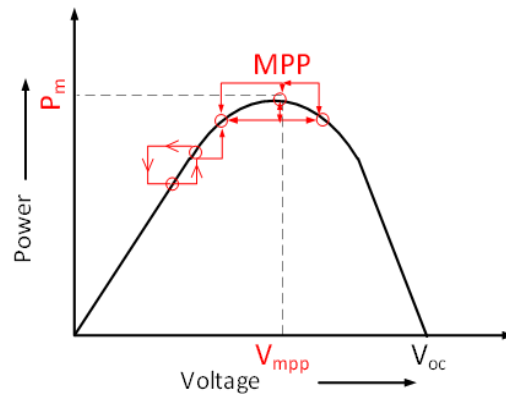
### 3.2.3 Modeling of MPPT Controlled Boost Converter

#### 3.2.3.1 MPPT Control

As the PV cell exhibits non-linear characteristics similar to diode characteristics. The output voltage of PV cell totally depends on the load resistance. In order to extract maximum power, maximum power point tracking (MPPT) algorithm is used. Several MPPT control techniques were proposed by different researchers [135–137]. From the literature Perturb & Observe (P&O) algorithm is selected for the study because of its robustness, easy implementation, and simple construction. The flow chart of the P&O MPPT algorithm and its graphical representation are shown in Figure. 3.7(a) and Figure. 3.7(b) of Figure. 3.7. The  $V_{mpp}$ ,  $P_m$  are the computed



(a) Flow chart of P & O algorithm



(b) P & O algorithm tracking for MPP

FIGURE 3.7: MPP control for boost converter of PV

voltage, power at MPP. The MPPT algorithm senses voltage ( $V_t$ ) and ( $i_t$ ) current output from the PV panel and calculates power ( $P_t$ ). The power computed is compared with the value of power from the previous state ( $P_{t-1}$ ) based on the conditions as stated in the flowchart of Figure. 3.7(a). Increment or decrement ( $\Delta V$ ) of the duty cycle is computed based on this process and is applied to the PV panel to modify the operating voltage. As the operating voltage is changed,

the output power of the PV panel is also changed accordingly. Small perturbations of ( $\Delta V$ ) are added to the system by continuous monitoring of output power and the process is continued till the MPP is reached which is graphically described in Figure. 3.7(b). The complete block diagram of PV generating system including all these elements is shown in Figure. 3.8.

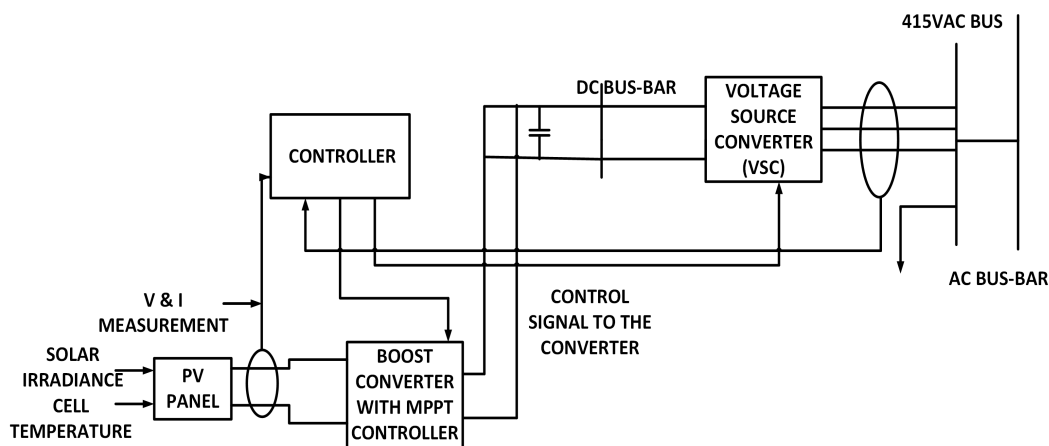


FIGURE 3.8: Block diagram of PV generating system

### 3.2.3.2 MPPT Controlled Boost Converter

The MG containing PV generating system is implemented with equation-based modeling in MATLAB, Simulink and is constructed under standard test conditions. The configuration of PV model consists of 6 panels connected in series and the output voltage of the configuration is  $6 \times 30.75 = 185$  V at MPP and the output power at MPP is obtained by multiplying with the current at MPP and is given by  $185 \times 8.04 = 1490$  W. i.e 1.5 kW. However, the output voltage from PV panel is low and in order to step up the output voltage of the PV system to the desired value, a boost converter is used. A boost converter is a power electronic device whose output voltage is greater than input DC voltage. The Boost converter consists of DC input voltage (i.e the output voltage from PV panel)  $V_0$ , IGBT switch, diode D, boost inductor L, and the filter capacitor C, as shown in Figure. 3.9. Operation of the boost converter is based on the continuity of the DC current through the inductor  $i_L$ .

The input DC voltage supplies energy to the inductor L. The MPPT algorithm ( $P\&O$ ) explained in 3.2.3.1 is used to track the MPP. The duty cycle of the boost converter is controlled to achieve

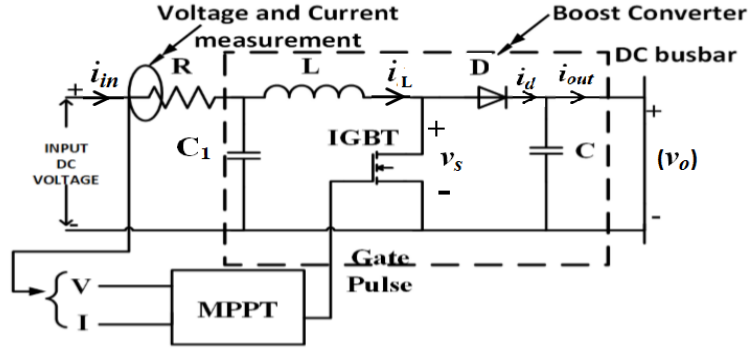


FIGURE 3.9: MPPT controlled boost converter of PV

desired output voltage. The equivalent circuit of the MPPT controlled boost converter of PV model is shown in the above Figure 3.9. When the switch (IGBT) is turned off, diode D is forward biased, and the energy stored in the L is delivered to the load or output circuit through the diode. Using Faraday's law for the boost inductor

$$V_i = (V_0 - V_i)(1 - D)T \quad (3.8)$$

where,  $D = \text{duty cycle} = \frac{t_{on}}{t_{on} + t_{off}} = \frac{t_{on}}{T}$ ,  $T = \text{Total time period of the switching}$ . From which the DC voltage transfer function turns out to be

$$\frac{V_0}{V_i} = \frac{1}{1 - D} \quad (3.9)$$

From (3.9) it is clear that the output voltage is greater than the input voltage. The boost converter is considered as operating in the Continuous Current Mode (CCM) [138]. The value of boost inductor (L) is calculated as :

$$L = \frac{V_i \times (V_0 - V_i)}{\Delta I_L \times f \times V_0} \quad (3.10)$$

where  $f = \text{switching frequency}$ ,  $\Delta I_L = \text{Inductor ripple current}$  and is given by:

$$\Delta I_L = 0.2 \times i_{omax} \times \frac{V_0}{V_i} \quad (3.11)$$



The value of the output capacitance ( $C$ ) is given by

$$C = \frac{i_{omax} \times D}{f \times \Delta V_0} \quad (3.12)$$

where  $i_{omax}$  = maximum output current,  $f$  = switching frequency and  $\Delta V_0$  = desired output voltage ripple. It is clear from the design of the boost converter that the value of boosted output voltage depends upon the duty cycle of IGBT switch. In order to achieve desired output voltage for the PV system with boost converter under consideration, the duty cycle of the boost converter is varied using MPPT algorithm. In order to extract maximum power, the PV has to be operated at the knee point i.e. MPP in the P-V characteristics of PV panel as shown in Figure. 3.7.

### 3.2.4 Simulation of PV Generating System

The two diode PV panel is modeled and simulated as described in section 3.2.2. The Simulink implementation of the equation based design of PV generation is shown in Figure. 3.10. The

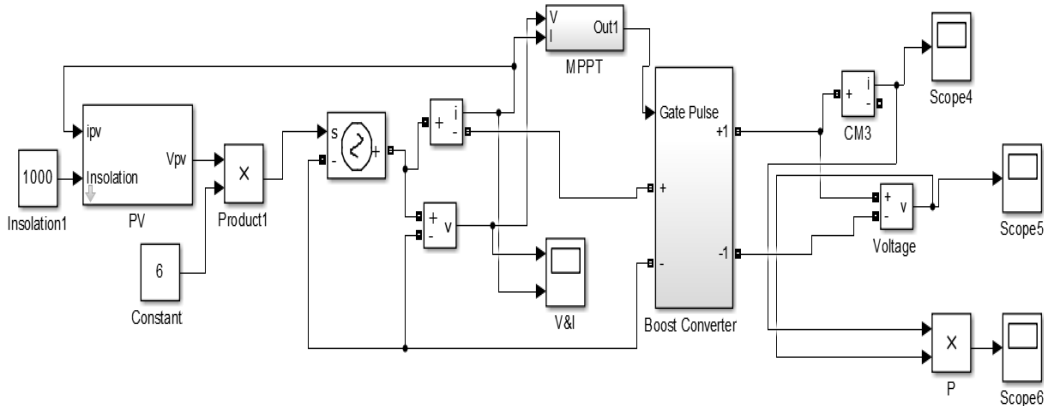


FIGURE 3.10: Simulink implementation of PV generation

electrical parameters are considered from the manufacture data sheet as shown in Table 3.5. In order to get a desired AC voltage of 415 V at common AC bus bar, PV output voltage is to be boosted upto an output voltage ( $V_0$ ) of 560 V from an input voltage of ( $V_i$ ) of 185 V. Accordingly the boost converter has been designed. The inductor ( $L$ ) and capacitor ( $C$ ) values of DC-DC boost converter computed are 8 mH and 100  $\mu$ F.  $\Delta I_L = 1.5$  A,  $\Delta V_0 = 2$  V,  $I_{0max} = 2.5$  A,  $D =$

50% and  $f_s = 10$  kHz.

The output of PV generation is shown in Figure. 3.11. The output voltage (30.5 V) of a single

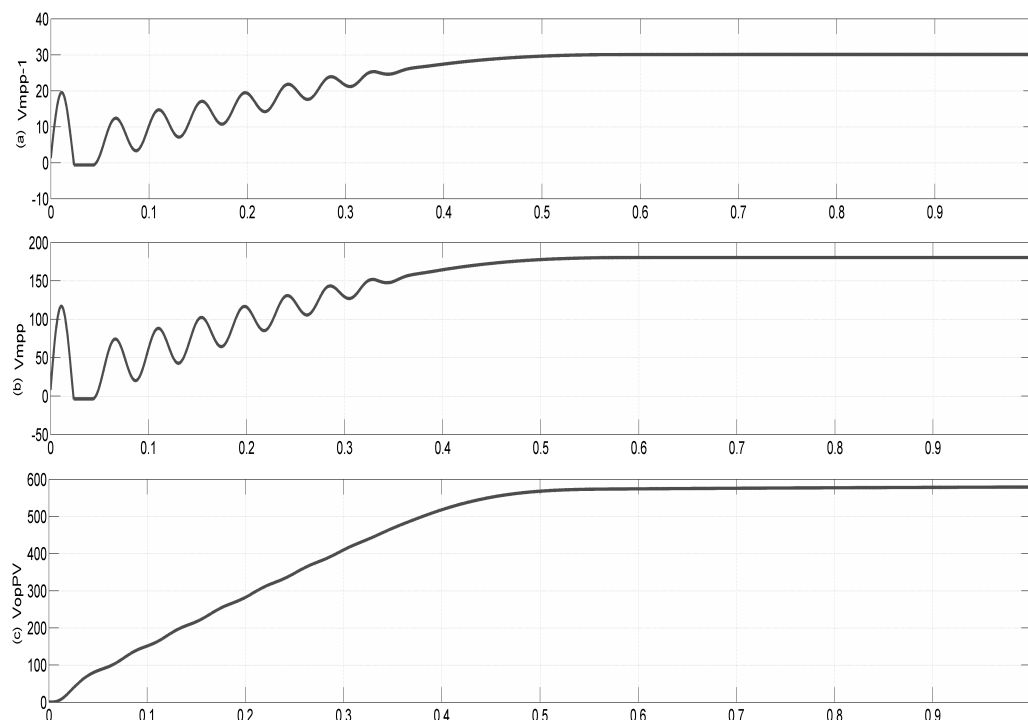


FIGURE 3.11: Output Voltage at different stages of PV generation

PV panel is represented in Figure. 3.11(a). Such 6 strings (PV panels) are connected in series and the resultant output (185 V) is shown in Figure. 3.11(b). However, the output is quite low. In order to get 415 V, AC (with the help of DC-AC converter) at common AC bus bar as per the block diagram in Figure 3.8, a DC equivalent voltage of 586 V is desired at the output terminal of PV system i.e., at the DC bus in Figure 3.8. This can be achieved by using a boost converter which steps up from 185 V DC voltage to 586 V. The boost converter modeling and design is discussed in 3.2.3.2 and 3.2.4. The output voltage of PV generating system is stepped up to the desired value (586 V) using the boost converter as shown in Figure. 3.11(c). The output DC voltage is further fed to a DC-AC converter to get a 3-phase, distribution level voltage of 415 V, 50 Hz. However, due to the intermittent nature of PV, it is always preferred to use another DG source which can complement the output voltage to maintain a constant AC at the common bus bar which in turn benefits the consumers of the MG with no interruption. In this regard, a Wind

Energy Conversion System (WECS) is used as second DG in the considered MG. The detailed operation of WECS is discussed in the next section.

### 3.3 WECS Based Generation

In the micro-grid network, it is especially difficult to support the critical load without uninterrupted power supply. Hence a wind energy conversion system is proposed in the construction of MG that maintains the controllable real and reactive power in the MG and to meet the power quality norms. Wind energy generation is a clean and inexhaustible energy providing a feasible solution to energy shortage. The micro wind power generation system is becoming more prominent with the increasing demand for power generation along with other connected DGs like PV. It also reduces the environmental pollution. However, the output power of micro wind generator is fluctuating and will affect the operation of the distribution network. The utility system cannot accept new generation without the strict condition of voltage regulation due to real power fluctuation and reactive power generation/absorption [139]. The industrial and commercial customers often operate the sensitive electronic equipment or critical load that cannot tolerate voltage sags, voltage swells, or loss of power, which moreover cause an interruption in life operating equipment or stoppage in industrial production. This requires some measure to mitigate the output fluctuation so as to keep the power quality in the distributed network. A few measures have been taken to overcome these challenges such as proper selection of a site for wind power generation, the design of wind turbine, power electronic controllers depending on the wind profile of the location. This requires an insight of wind power generation along with major elements including its operation. The following subsections provide the modeling of WECS in detail.

#### 3.3.1 Modeling of WECS

The wind energy conversion system (WECS) consists of Wind turbine, Permanent Magnet Synchronous Generator (PMSG), Diode rectifier, Boost converter, MPPT algorithm. The block

diagram of WECS is shown in Figure. 3.12. The modeling of WECS of the MG includes modeling of a wind turbine, boost Converter and MPPT algorithm and is explained as follows:

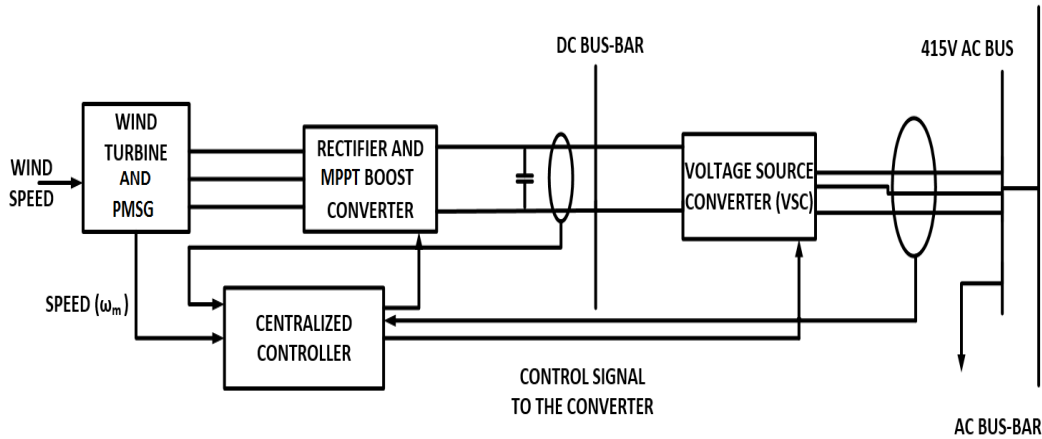


FIGURE 3.12: Block diagram of WECS generation

### 3.3.1.1 Modeling of Wind Turbine

The wind turbine converts the wind's kinetic energy into mechanical energy with a rotor with two or more blades mechanically coupled to the electrical generator. The wind turbines are placed on the tall towers in order to enhance the wind energy capture. The height of the tower and the size of the wind turbine varies with the generation capacity of the wind power generation system. The power extracted by the blades is expressed as a fraction of the upstream wind power in watts given by (3.13)

$$P_0 = \frac{1}{2} \rho A V^3 C_p \quad (3.13)$$

where  $P_0$  = mechanical power extracted by the rotor, i.e., the turbine output power,  $\rho$  air density ( $\text{Kg}/\text{m}^3$ ),  $A$  = area swept by the rotor blades ( $\text{m}^2$ ),  $V$  = velocity of the air ( $\text{m}/\text{s}$ ), and  $C_p$  = Power Coefficient. The power coefficients  $C_p$  is the most important parameter in the case of power regulation. It is a non-linear function whose value is unique to each turbine type and is a function of wind speed that the turbine is operating. The model of  $C_p$  is a function of the tip speed ratio ( $\lambda$ ) and the blade pitch angle  $\theta$  in degrees and is given by (3.14)

$$C_p(\lambda, \theta) = C_1 \left( C_2 \frac{1}{\beta} - C_3 \beta \theta - C_4 \theta^x - C_5 \right) e^{-C_6 \frac{1}{\beta}} \quad (3.14)$$

where the values of the coefficients  $C_1 - (C_6$  and 'x' depend on turbine type,  $\theta$  is defined as the angle between the plane of rotation and the blade cross section chord and  $\beta$  is defined by (3.15)

$$\frac{1}{\beta} = \frac{1}{\lambda + 0.08\theta} - \frac{0.035}{1 + \theta^3} \quad (3.15)$$

The function  $C_p$  is implemented in MATLAB, Simulink using (3.14)-(3.15) and the relationship between power coefficient ( $C_p$ ) and tip-speed ratio ( $\lambda$ ) is simulated and the graphically representation of the simulation results is shown in Figure. 3.13. The Betz limit says that wind turbine can convert to above (59.3%) of the kinetic energy of the wind into mechanical energy i.e. rotation of turbine, i.e.  $C_{pmax} = 0.59$ . The maximum wind power is to convert into mechanical

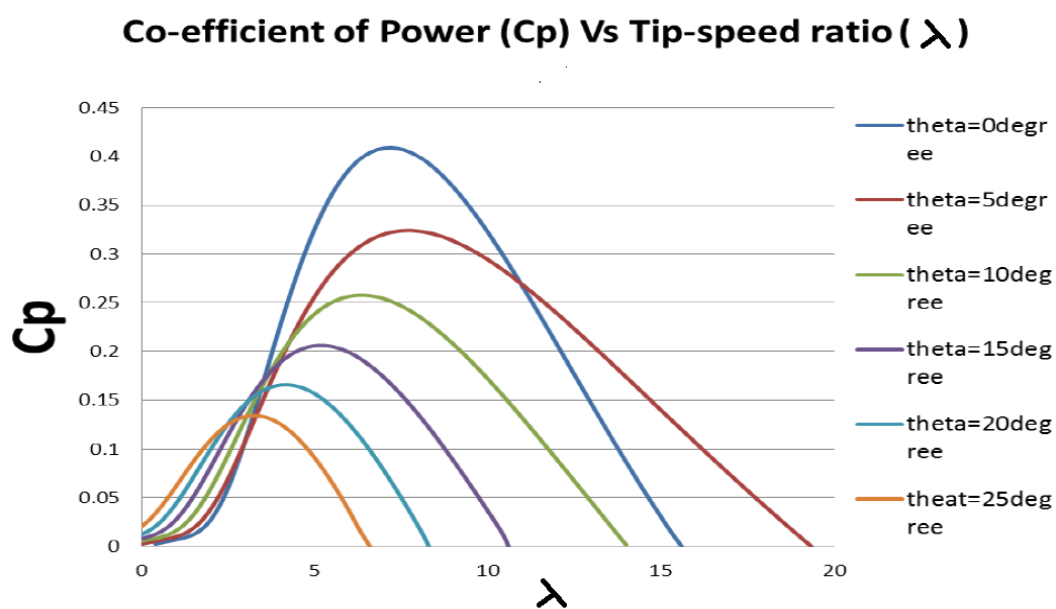


FIGURE 3.13: Simulated plot of Power Co-efficient ( $C_p$ ) Vs Tip-Speed ratio ( $\lambda$ )

power to produce the required mechanical torque to drive the PMSG for power generation. The relation between the mechanical torque ( $T_m$ ) and mechanical power output ( $P_m$ ) of the wind turbine is given by(3.16) [140],

$$T_m = \frac{P_m}{\omega_m} \quad (3.16)$$

where  $\omega_m$  = rotor angular speed (rad/s).

$$\omega_m = \frac{\lambda V}{R} \quad (3.17)$$

where  $R$  is the wind turbine rotor radius in meters (m),  $\lambda$  is the tip-speed ratio. Using the basic knowledge of mathematical modeling of wind turbine the equation based model of wind turbine [140] is implemented in MATLAB, Simulink and the parameters considered for the design are  $R = 1.25$  m, length of blade  $L = 2.5$  m,  $A = 6.25$  m<sup>2</sup>,  $\rho = 1.225$  kg/m<sup>3</sup>.

### 3.3.1.2 Equation Based Modeling of PMSG

The equation based model of PMSG in dq reference frame is given by (3.18), (3.19)

$$\frac{di_d}{dt} = \frac{1}{L_d}(-R_s i_d + \omega_e L_q i_q + V_d) \quad (3.18)$$

$$\frac{di_q}{dt} = \frac{1}{L_q}(-R_s i_q + \omega_e [L_d i_q + \lambda_0] + V_q) \quad (3.19)$$

where,  $R_s$  – Stator Resistance ( $\Omega$ ),  $L_d$ ,  $L_q$  – Inductance of the generator on d and q-axis (H),  $\lambda_0$  – magnetic flux of Permanent Magnet (wb),  $i_d$ ,  $i_q$  – d and q- axis currents (A),  $V_d$ ,  $V_q$  – voltage across the load on d and q- axis (V),  $\omega_e$  – speed of generator (rad/s) =  $P\omega_m$ ,  $P$  = number of pole pairs of generator. Assuming the inductance of generator on d, q- axis as

$$L_d = L_q = L \quad (3.20)$$

substituting (3.20) in (3.19),(3.18)

$$\frac{di_d}{dt} = -\frac{R_s i_d}{L} + \omega_e i_q + \frac{V_d}{L} \quad (3.21)$$

$$\frac{di_q}{dt} = -\frac{R_s i_q}{L} + \omega_e \left(i_q + \frac{\lambda_0}{L}\right) + \frac{V_q}{L} \quad (3.22)$$

The q-axis counter electric potential  $e_q = \omega_e \lambda_0$  and the d-axis counter electric potential  $e_d = 0$  and the equivalent circuit for both d and q axis derived from (3.21), (3.22) are shown in Figure. 3.14(a), Figure. 3.14(b). Hence the electric torque produced by PMSG is

$$T_e = \frac{3}{2} \left(\frac{P}{2}\right) (\lambda_0 i_q - \lambda_q i_d) \quad (3.23)$$

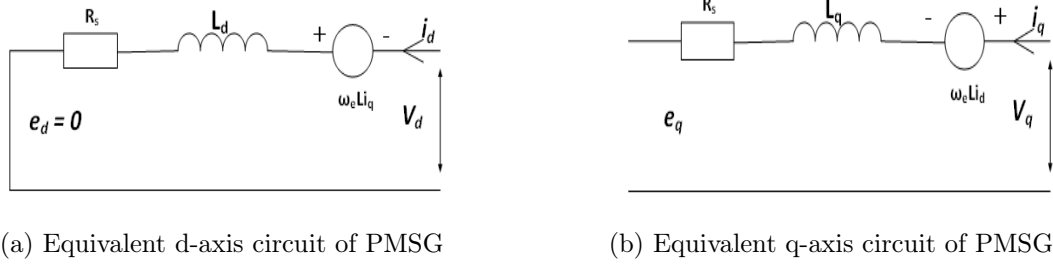


FIGURE 3.14: Modeling of PMSG

Re-writing (3.23) as (3.24)

$$T_e = \frac{3}{2} \left( \frac{P}{2} \right) (\lambda_0 i_q + (L_d - L_q) i_q i_d) \quad (3.24)$$

As both d and q- axis inductances are equal, hence the electromagnetic torque (3.24) can be expressed in terms of  $i_q$  as

$$T_e = 1.5 P i_q \lambda_0 \quad (3.25)$$

The electrical parameters for the PMSG are Stator Resistance  $R_s = 2.875 \Omega$ ,  $L_d = 0.0085 \text{ H}$ ,  $L_q = 0.0085 \text{ H}$ ,  $\lambda_0 = 0.175 \text{ Wb}$ , Pole Pairs  $p = 2$ , Moment of inertia  $J = 0.0008 \text{ Kg } m^2$ . Using the knowledge of mathematical modeling of PMSG an equation based model of PMSG is implemented in the Simulink using (3.18), (3.19), and (3.25) as shown in the Figure. 3.15. The output voltage from the PMSG is not a constant value as its variation depends on the variation in wind speed. In order to maintain constant output voltage across the load the variable output voltage from the PMSG is rectified using diode bridge rectifier and the rectified voltage is stepped up to the required level and maintained constant using a boost converter. The modeling of boost converter will be discussed in detail.

### 3.3.1.3 MPPT Controlled Boost Converter

PMSG electrical generator coupled to Wind turbine converts mechanical energy from a wind turbine into electrical energy. The output voltage and frequency depend upon the speed at which wind turbine rotates i.e wind speed. In large wind turbines, in order to maintain a speed

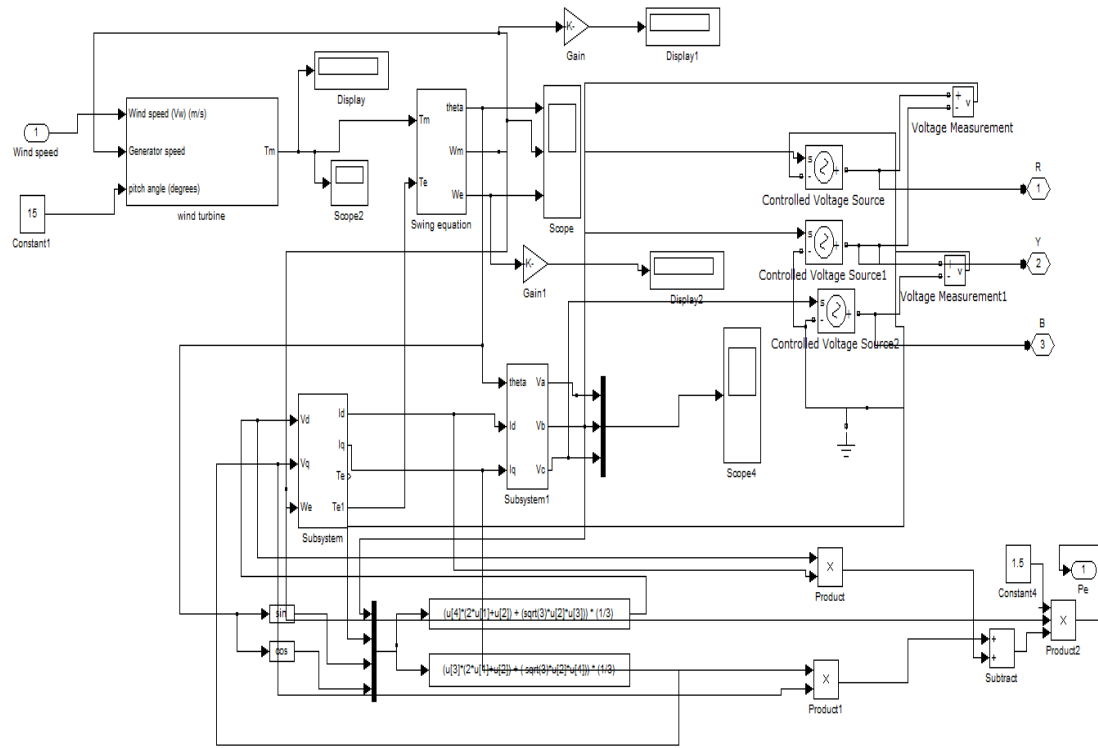


FIGURE 3.15: Simulink model of WECS

of the generator constant gear-box assembly is utilized. For low wind speed applications, the gear-box assembly will decrease the efficiency as the gearbox assembly is bulky and it requires regular maintains and it adds cost to the system. In order to overcome these direct driven wind turbines are used for low wind application. In order to maintain the output voltage and frequency constant obtained from such wind turbine the output voltage of the electrical generator i.e. PMSG is first converted into DC, this DC voltage is boosted up to the required voltage level using boost converter as shown in the Figure. 3.16(a). The MPPT controlled boost converter is implemented to track the MPP continuously. The duty cycle of the boost converter is controlled by MPPT algorithm i.e. Hill Climb Search (HCS) algorithm. The graphical representation of MPPT is shown in Figure. 3.16(b).The control strategy of HCS algorithm is to sense output voltage, current from the diode rectifier and speed from the PMSG to compute power. Later the calculated power is compared with respect to the power for the corresponding speed of PMSG. In order to achieve MPP the duty cycle of the boost converter is automatically varied and thus the desired output voltage irrespective of wind speed can be achieved as shown in Figure. 3.16(c). The mathematical modeling of the boost converter is similar to the modeling of boost converter



discussed in 3.2.3.2.

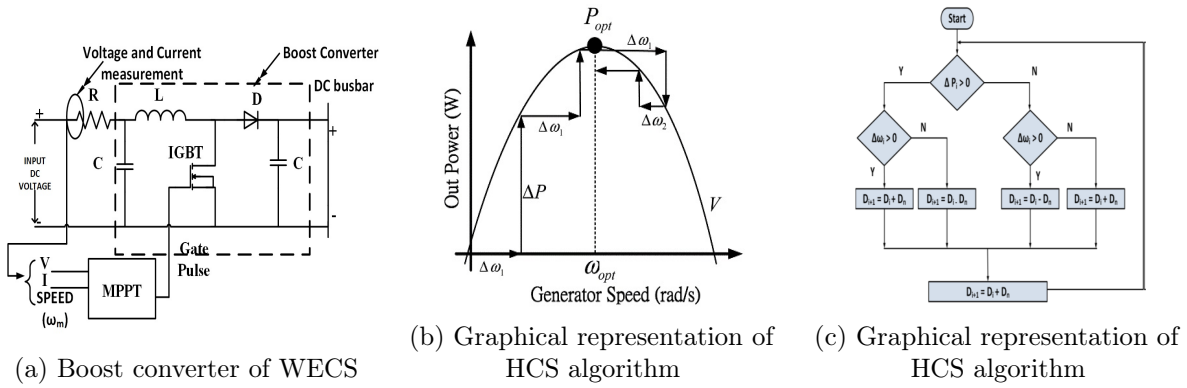


FIGURE 3.16: MPPT controlled boost converter of WECS

### 3.3.2 WECS Simulation

Based on complete modeling of WECS presented in 3.3.1, including modeling of wind turbine in 3.3.1.1, equation based modeling of PMSG in 3.3.1.2, MPPT controlled boost converter in 3.3.1.3, corresponding simulink model has been developed in MATLAB. The output voltage from

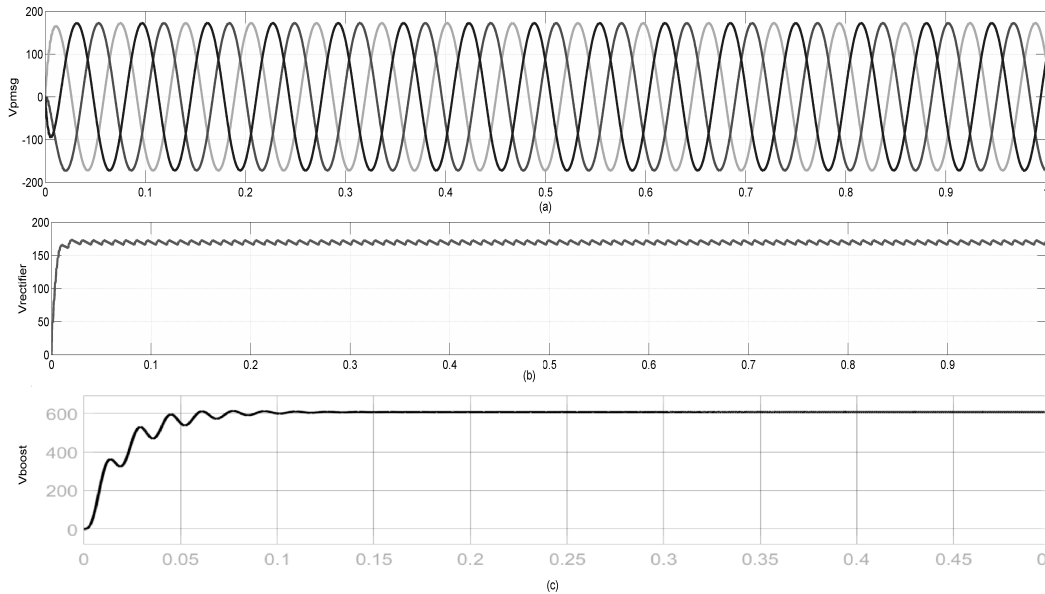


FIGURE 3.17: Output voltages at different stages of WECS

PMSG is 180 V, (L-L Voltage) as shown in Figure. 3.17(a). Instead of using a gearbox to step up the voltage, it is preferred to convert to DC voltage using diode rectifier and then stepping-up using boost converter [141]. From boost converter, the stepped-up DC voltage is brought to a

common DC bus bar. The voltage from DC bus bar is converted to AC using a Voltage Source Inverter (VSI) to get the desired 3-phase, distribution level voltage of 415 V at common AC bus. The voltage from PMSG is rectified to 165-170 V as shown in Figure. 3.17(b). The obtained DC voltage can be further boosted up to different values by designing the boost converter as discussed in 3.2.3.2. To generate 3-phase, 415 V, AC output voltage, corresponding stepped up DC voltage of 580 V from the boost converter is required and the obtained boost converter output is shown in the Figure. 3.17(c). The VSI used is 3-phase 3-arm 6 pulse IGBT bridge inverter to develop 3-phase, 415V distribution level voltage. The output voltages in terms of RMS at different stages of WECS are also shown in Figure. 3.18. The 125 V RMS voltage from

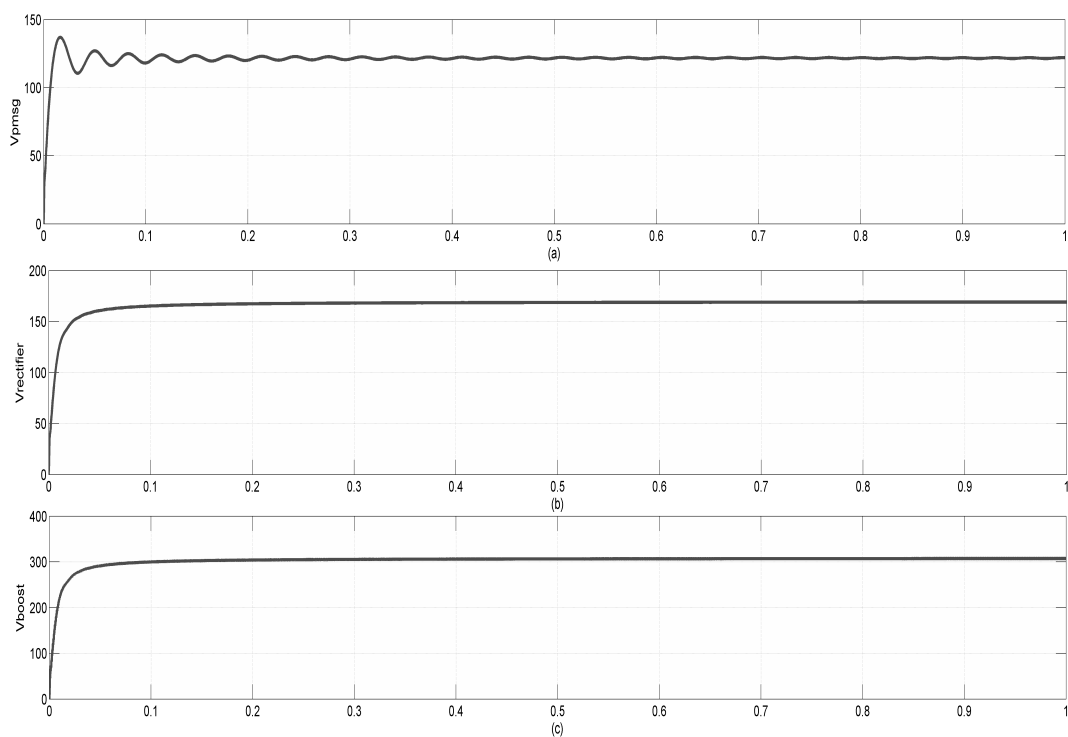


FIGURE 3.18: Output voltages (RMS) at different stages of WECS

PMSG is shown in Figure. 3.18(a) which is converted to 163 V DC is shown in Figure. 3.18(b). The boost converter is further used to step up this DC voltage to 280-300 V is shown in Figure. 3.18(c).

### 3.4 PV-WECS Microgrid Simulation using Real-Time Data

The MG is designed to deliver a 3-phase distribution voltage of 415V, 50 Hz at the common AC bus. The developed PV-Wind MG has been analyzed in real time for the environmental conditions measured at location BITS-Pilani, Hyderabad campus, TS, India. The longitude and latitude of the location are 17.54650 N, 78.57250 E. The solar irradiation and wind profile for the location are measured using Weather Monitoring System (WMS) installed in the campus as shown in Figure. 3.19. The record of solar insolation and wind speed is observed from the data log sheet of WMS is given in Figure. 3.19(a). The real-time value of the wind speed and wind direction is measured using anemometer as shown in Figure. 3.19(b) and the real-time data of solar irradiance level is measured using the solar irradiance measurement is shown in Figure 3.19(c).

In Figure. 3.20(a), Figure. 3.20(b), Figure. 3.21 are the graphical representation of the real-time

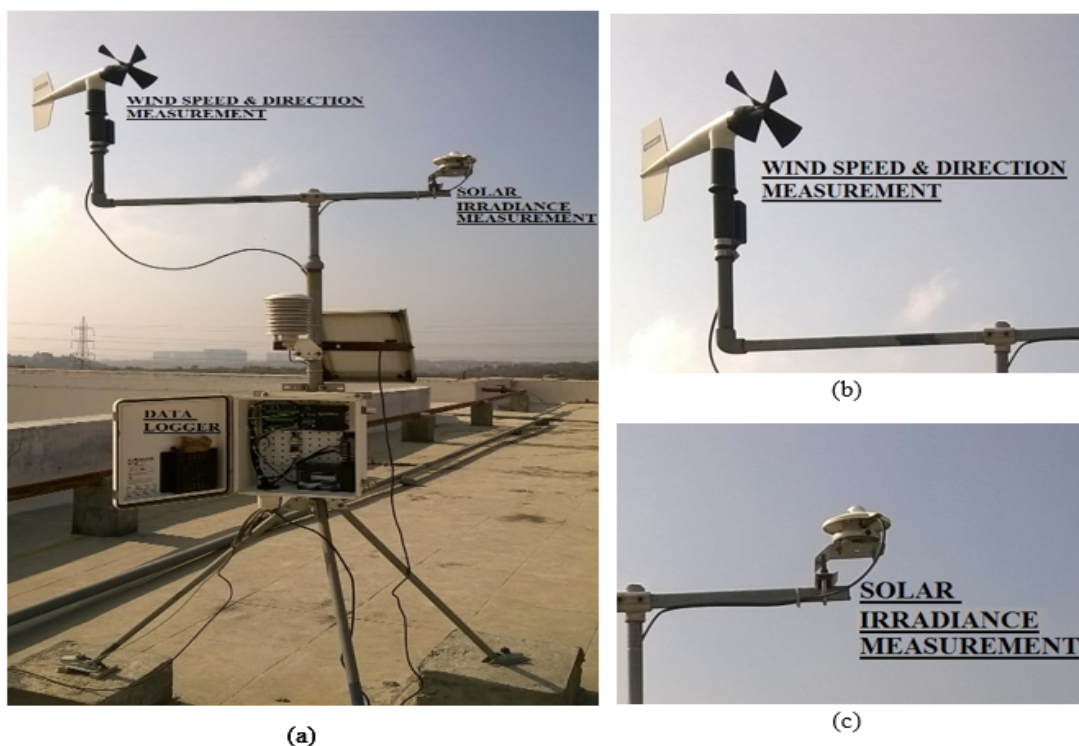


FIGURE 3.19: Weather Monitoring System (WMS) for extracting real time data

data of wind speed measured at the location. Figure. 3.20(a) shows hourly average and maximum wind speed for a day in the month of July. Figure. 3.20(b) gives that the monthly average

is above 3 m/s and touching 5 m/s and maximum wind speed is between 8 m/s to 14 m/s for a month of July. Similarly, Figure. 3.21 gives a daily average and maximum speed per day over the year of 2017. The wind profile is quite good for low wind speed generation with average wind speed above 3 m/s and with the average maximum wind speed of 12 m/s. It can be clearly comprehended that wind profile is fair enough to build a direct driven wind power generation system with average wind speed above 4m/s and maximum wind speed is stable at 11 m/s. The graphical representation of solar irradiation levels per day, month, year for

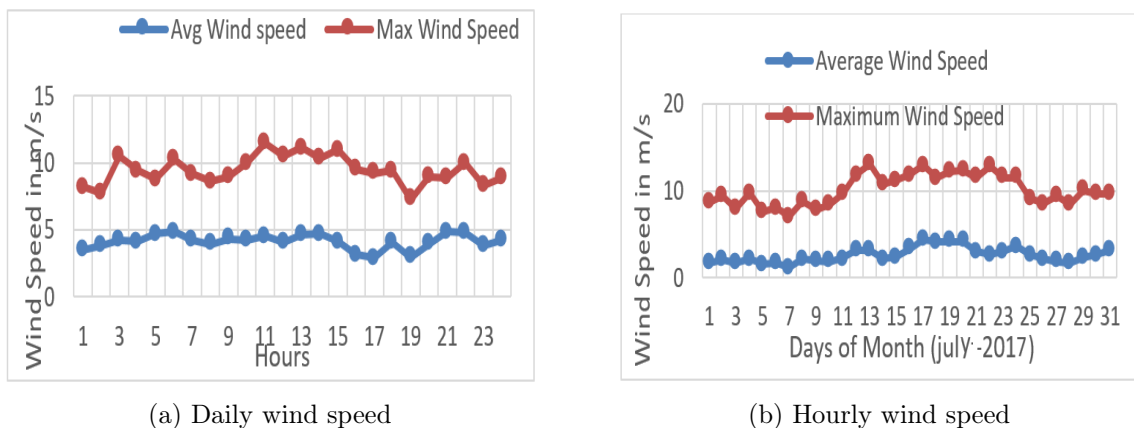


FIGURE 3.20: Wind profile from WMS

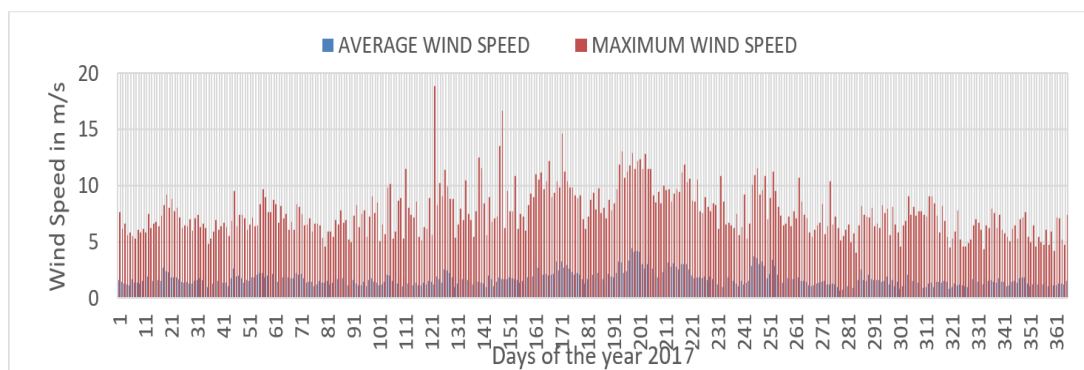


FIGURE 3.21: Average and maximum wind speed for the year 2017

the year 2017 are shown in Figure. 3.22(a), Figure. 3.22(b) and Figure. 3.23. Figure. 3.22(a) shows a graphical representation of hourly solar irradiance for a day in the month of September 2017 and Figure. 3.22(b) shows the graphical representation of solar irradiance for the month of September 2017 with very good solar irradiation levels over the month with the peak hour solar irradiation touching  $1400 \text{ W/m}^2$ . From the Figure. 3.23, it is clear that the location has

a good solar energy over the year with maximum solar irradiations level touching  $1500 \text{ W/m}^2$  with average solar irradiation level around  $600 \text{ W/m}^2$ . It can be clinched that the location under consideration has a good solar irradiation level from 8 am to 6 pm with minimum irradiation of  $600 \text{ W/m}^2$  and maximum value touching  $1400 \text{ W/m}^2$ . Utilizing this real-time data of wind speed and solar irradiation analyzed for the location, the PV-Wind microgrid has been simulated. The equivalent period per hour, day and month are considered as 1 sec for simulation purpose. Later the variations in the output voltage and active and reactive power flow in each DG due to the continuous varying behavior of these parameters are also analyzed in the next section.

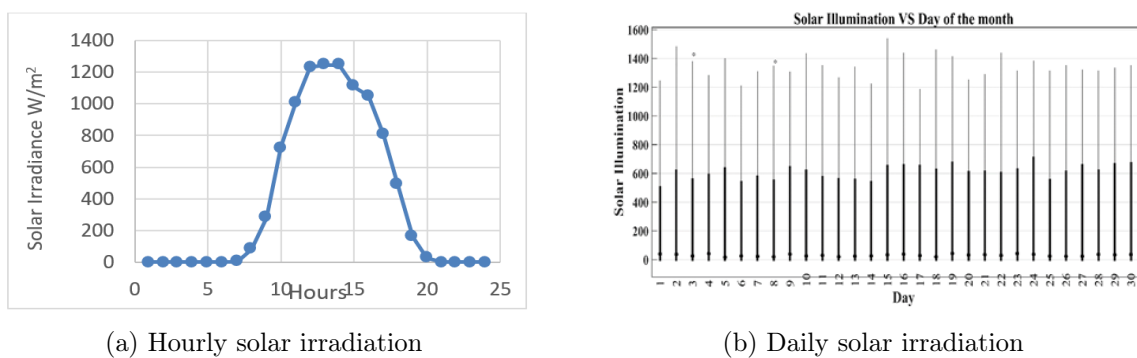


FIGURE 3.22: Solar insolation profile from WMS

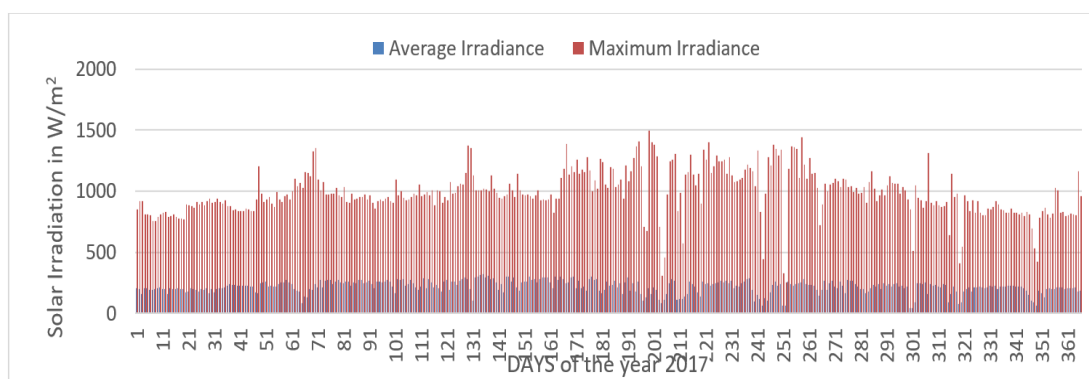


FIGURE 3.23: Average and Maximum solar irradiation for the year 2017

### 3.5 Microgrid Power Quality Issues

An MG containing PV-wind MG generating system is implemented in Simulink / MATLAB environment by appropriately modeling the DG sources, MPPT controllers, Boost converters

and the DC bus as shown in the Figure. 3.24. The developed system along with its controllers

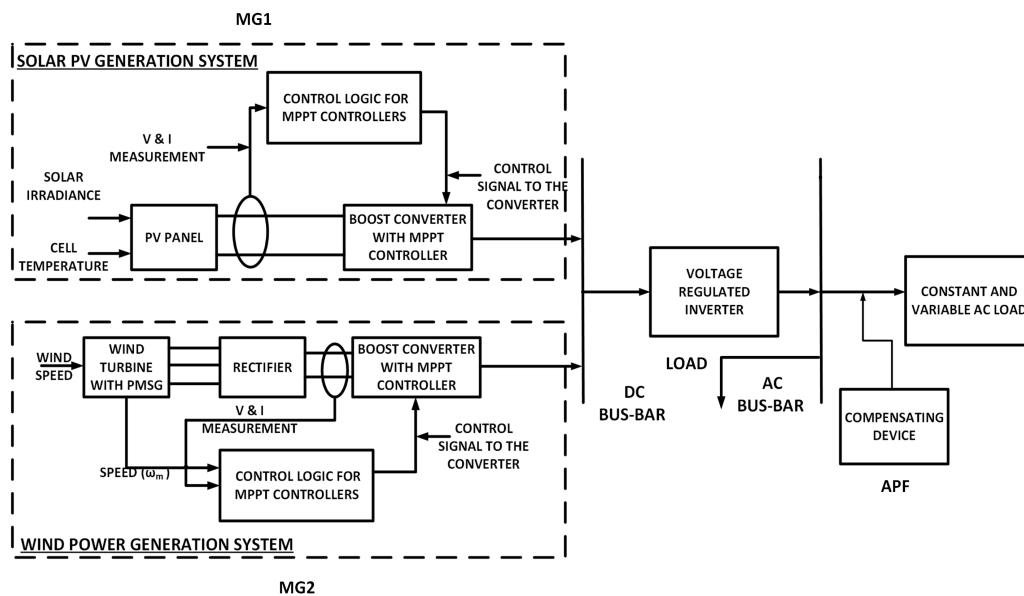


FIGURE 3.24: Block diagram of PV-WECS AC microgrid

has been investigated for the real-time data. The continuous variations in the solar irradiation and wind speed are observed which makes the output voltage varying in nature and causes many power quality problems including reactive power compensation. The usage of power converters in MG offers vast benefits like optimal operation and flexible control of the power apparatus and systems [142]. However, they create a plethora of power quality problems [53, 54, 68, 143, 144]. These issues may arise due to intermittent nature of the DGs connected to the MG, loads that demand reactive power, usage of high-speed power electronic loads that pollutes the entire system with harmonics.

As mentioned earlier, that any kind of power quality disturbance is related to the handling of the reactive power flow in the system with a corresponding change (loss) of active power. In this regard, the variable solar insolation and wind speed with respect to time which in turn cause varying output voltage, active and reactive power flows in each DG is observed and analyzed. The output voltage and active power responses in PV generating system due to the variation in solar irradiation within a range of 600-1000 W/m<sup>2</sup> for a duration of 1 sec are shown in the Figure. 3.25. Similarly, the output voltage, P, and Q responses in case of WECS due to the change in wind speed within a range of 8-12 m/s for a duration of 1 sec is shown in the Figure. 3.26.

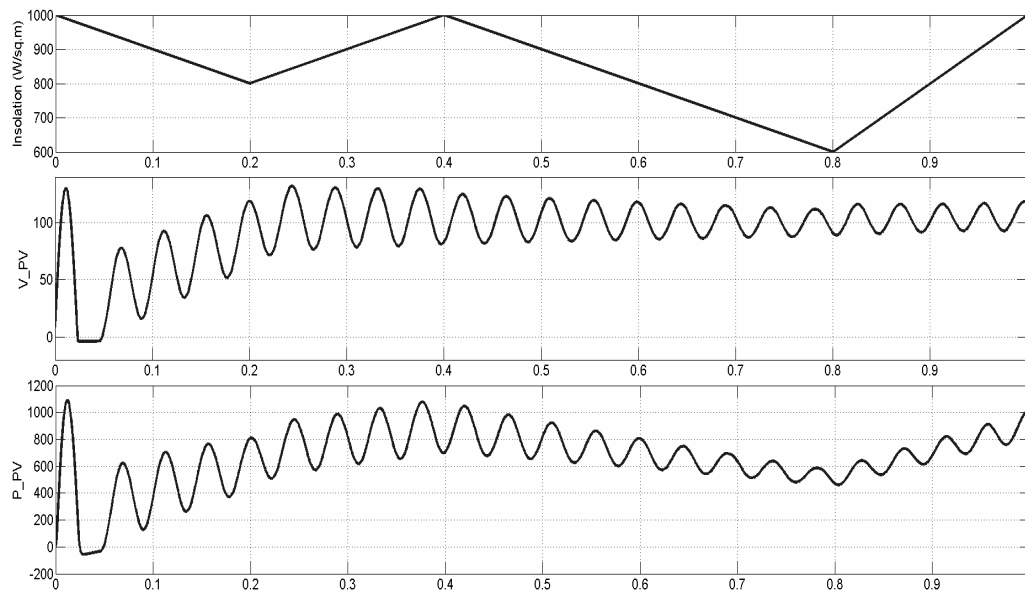


FIGURE 3.25: Voltage &amp; P variation due to change in solar insolation

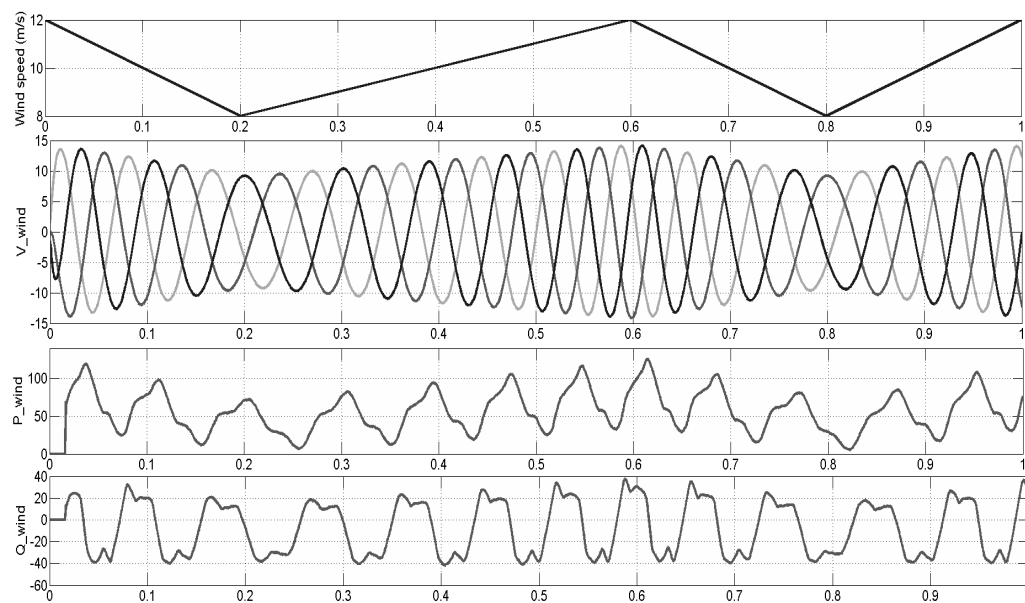


FIGURE 3.26: Voltage, P &amp; Q variation due to change in wind speed

Similarly, due to the frequent variations of the nature of loads (harmonic and reactive) connected, power quality issues are observed concluding the requirement of reactive power compensation in the MG. The corresponding changes in the output voltage in the form of a sag, swell, flicker due to both supply and load disturbances are shown in Figure. 3.27, Figure. 3.28 and Figure. 3.29. The variations in the supply voltage are approximated as  $\pm 21\%$  in the output voltage that gives a dip or rises 87.5 V as shown in the Figure. 3.27, Figure. 3.28. The simulations are carried

for a period of 1 sec, in which sag/swell is observed for 0.2 to 0.5 sec. Due to this the output voltage of 330 V is decreased to 242.5 V when there is sag, increased to 417.5 V when there is swell in the system. However, the flicker in the voltage from 0.1-0.3 sec is also observed. Due to the occurrence of flicker, the output voltage is changing continuously from 229.5 V to 402.5 V as shown in the Figure. 3.29.

Later the MG is connected to a non linear load to analyse its performance. A load containing a

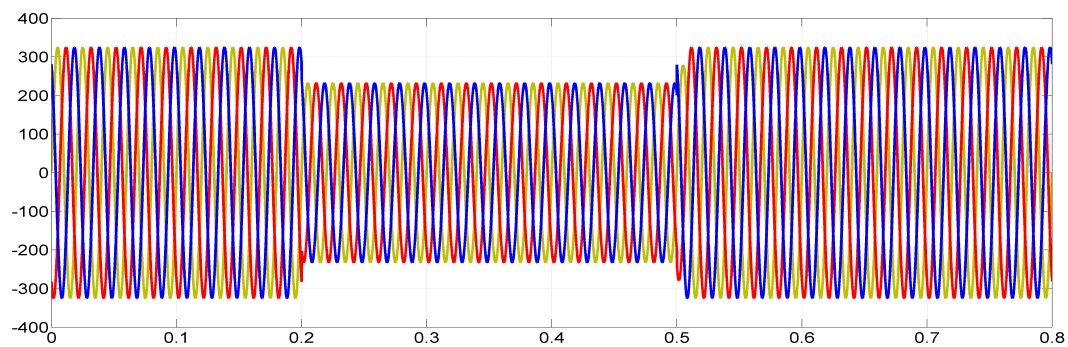


FIGURE 3.27: Sag in output voltage due to change in supply/load

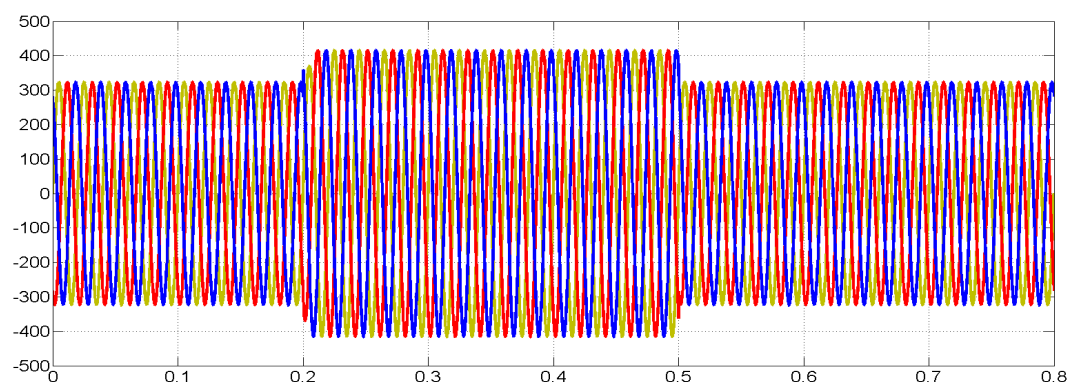


FIGURE 3.28: Swell in output voltage due to change in supply/load

3-phase full bridge diode rectifier delivering a RL load of  $10 \Omega + 0.15 \text{ mH}$  combined with a series RL load of  $0.4 \Omega + 15 \text{ mH}$  is connected to the MG. Load voltage containing many harmonics are observed as shown in the Figure 3.30. A THD of 24.48% is present in the resultant voltage as shown in the Figure 3.31. These harmonics in the voltage are to mitigated otherwise starts flowing towards MG supply and lead to rise in the supply currents. Similarly, the performance of MG is also analyzed for symmetrical and unsymmetrical faults. The MG is connected to a 3-phase resistive load of 1 kW along with an inductive load of 600 VAR. Different faults LG,



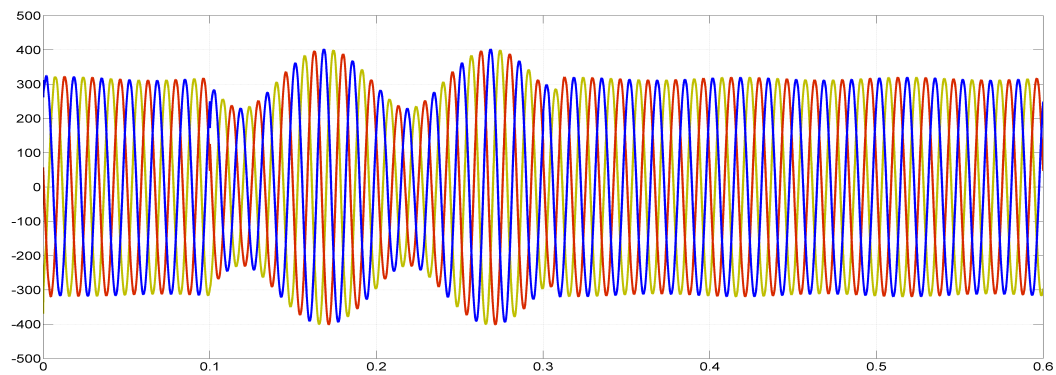


FIGURE 3.29: Flicker in output voltage due to change in supply and load

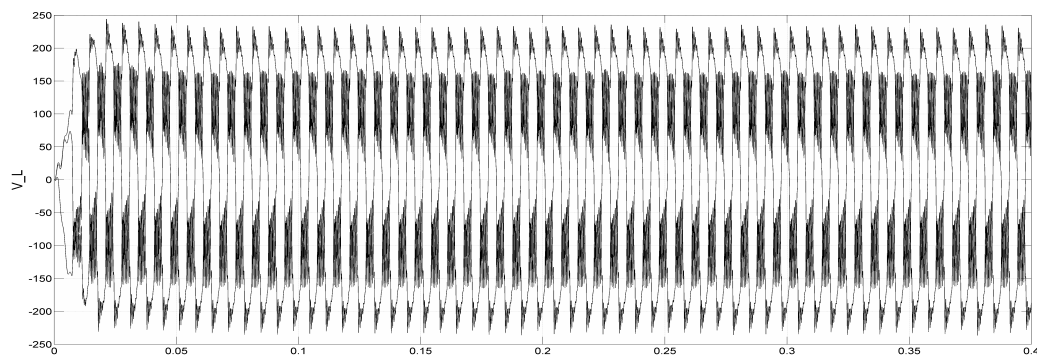


FIGURE 3.30: Harmonic load voltage

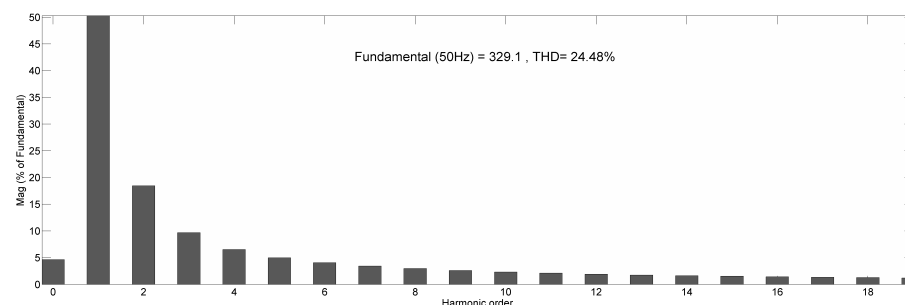


FIGURE 3.31: Harmonics in load voltage due to non-linear load

LLG and LLLG faults are simulated in the MG during 0.15 sec - 0.25 sec. The corresponding load current and voltage profiles are shown in Figure. 3.32 and Figure. 3.33. The actual load voltage without any fault is 415 V L-L. However, the voltage of phase-a in case of LG fault, voltages of phase a,b in case of LLG faults and all a,b,c phase voltages in case of LLLG fault are zero as shown in the Figure. 3.33 when the respective faults occurred in the MG. Similarly, the corresponding currents become very high and raised almost up to 250-300 A as shown in Figure. 3.33, where the actual load current without any fault is 2-3 A, i.e, the short-circuit current due to

these faults, is increased almost 100 times to that of actual value. This high current may damage the sensitive equipment that is connected to the MG. Hence, this high current is required to be limited to a lower value to ensure the safety of the MG equipment.

When an unbalanced load (i.e. three different loads in three phases) is connected to the MG

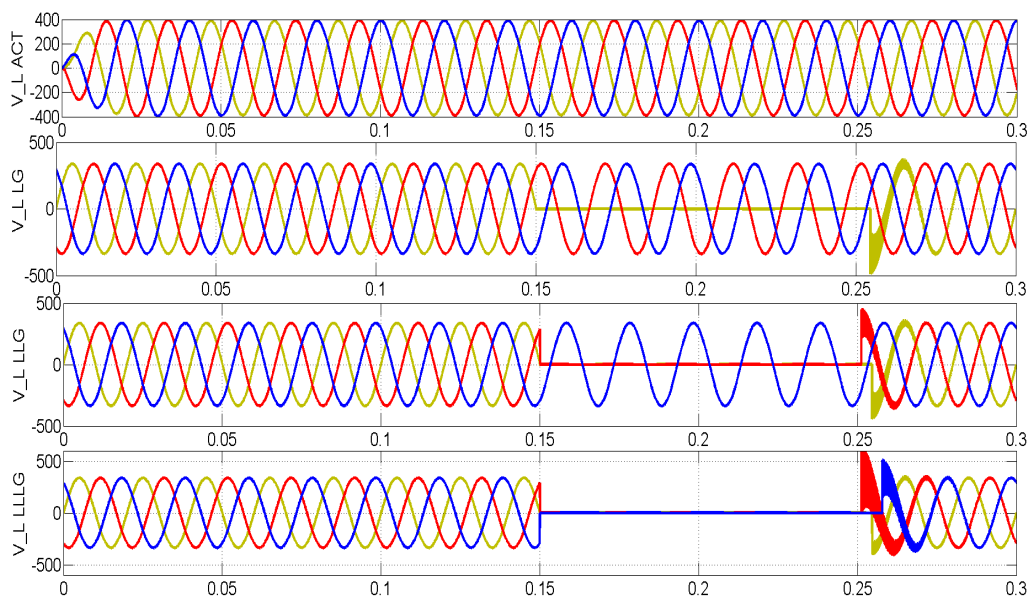


FIGURE 3.32: Load voltage profile due to various line faults in MG

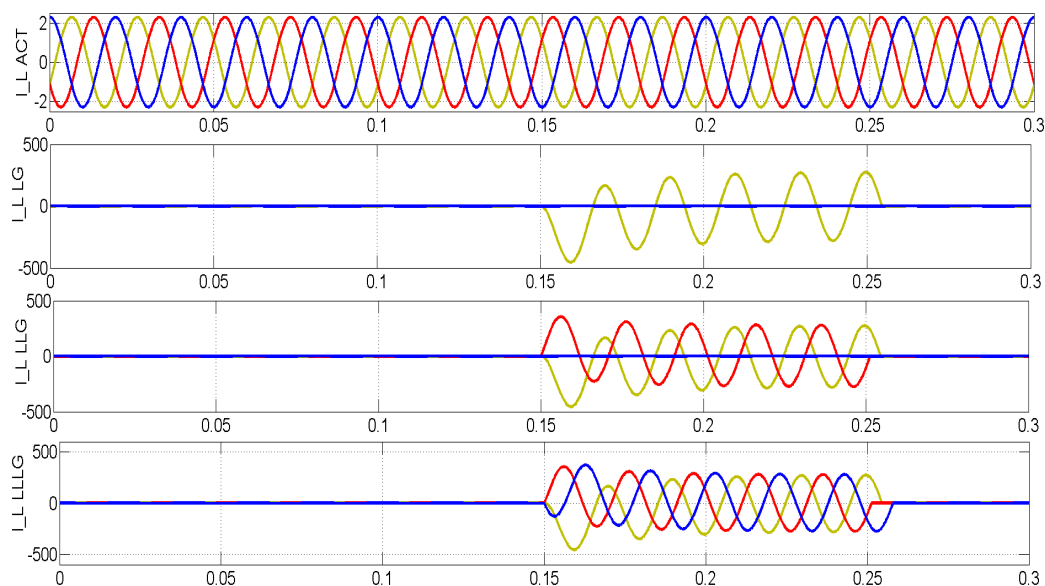


FIGURE 3.33: Current profile due to various line faults in MG

along with a nonlinear load. As a resultant load current becomes unbalanced which in turn flows towards the source and makes the currents at the source also unbalanced. In turn, the circulating currents

in the neutral are also raised. The unbalanced load current  $I_L$  and neutral circulating currents  $I_N$  are shown in Figure 3.34. The flow of unbalance and circulating currents due to this load unbalance is observed for a period of 0.1 sec. In order to avoid the flow of these circulating currents towards source, unbalance and neutral compensation is required. Later, to evaluate

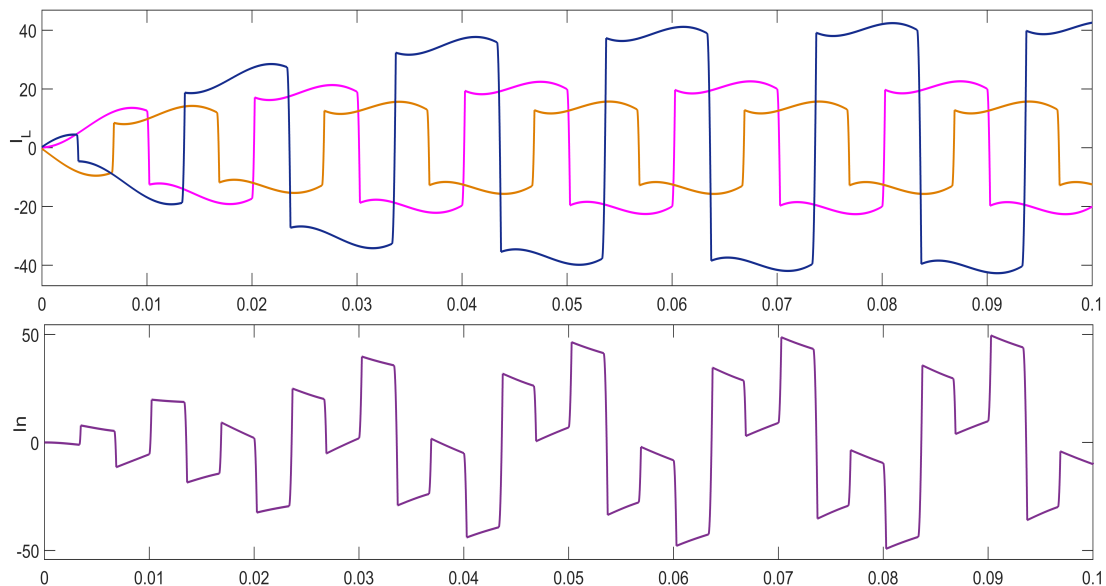


FIGURE 3.34: Flow of unbalance and circulating currents due to unbalanced load in MG

the performance of MG for current harmonics, another nonlinear load that gives high current harmonics is connected to the MG. When it is connected, the response of source current is shown in Figure 5.19 which is harmonic in nature. The THD of 150.84% is observed in source current as shown in Figure 5.20. Similarly, the power factor (p.f) of the system is also observed as

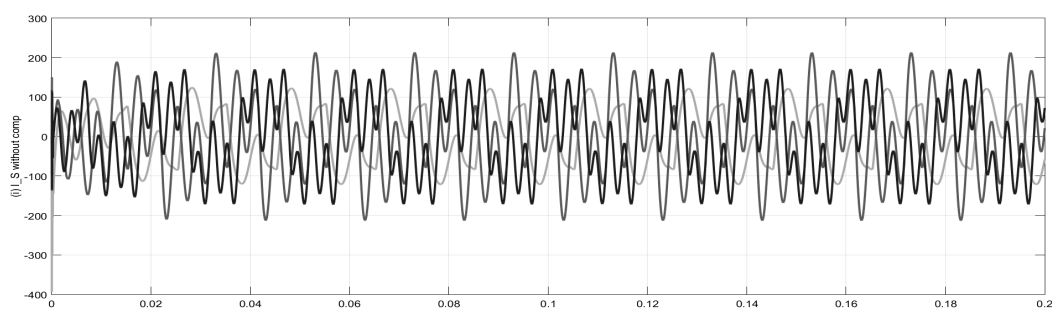


FIGURE 3.35: Source current with harmonics

shown in the Figure. 3.37. The reference power factor without any change in the load voltage is shown as  $pf_{ref}$ . When there is a dip in the load voltage with a disturbance in supply/load, the p.f of the system is decreased below the reference as shown in  $pf_{sag}$ . The increase in the

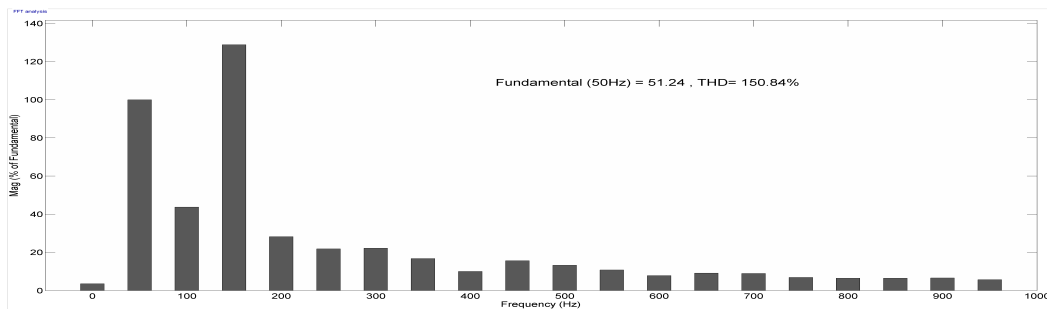


FIGURE 3.36: Source current with harmonics

load voltage with a disturbance in supply/load, the p.f of the system is increased above the reference as shown in  $pf_{swell}$ . The p.f due to simultaneous sag/swell is given by  $pf_{sagswell}$ . In all the cases, the p.f is varying due to system/load changes in the MG and is not maintained stably. In this regard, to mitigate all these concerned issues and also to improve the PQ of the MG,

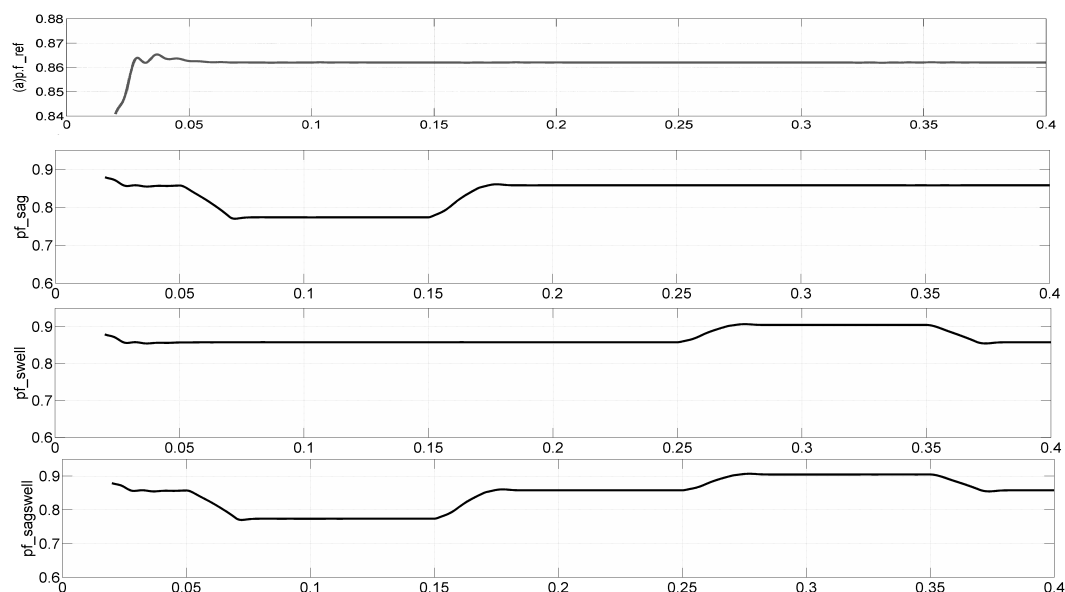


FIGURE 3.37: p.f variations due to change in voltage disturbances

compensation is required. In this regard, a review has been made and presented in Chapter. 2 on the required compensation against the aforementioned issues using various control techniques, algorithms, and devices. The survey recommended the implementation of a compensating device that can mitigate all the power quality issues in the microgrid. From the survey also suggested the application of custom power device with active filter topology can act as a power quality compensator and will be a powerful solution to any kind of power quality problem that occurs in

the microgrid. Hence, with this motivation modeling, design and implementation of different custom power devices in a microgrid are presented in the next chapters.

### 3.6 Conclusion

A microgrid with two DG sources connected to a common AC bus is considered in this chapter. The two DG sources (DG1 and DG2) are: a PV generation source and a wind generation source. An accurate model is selected for analyzing the performance of PV based generation and wind energy conversion system (WECS) under different varying conditions. A PV cell based on the two-diode model is considered in the construction of PV based DG1. The PV based DG is developed with equation-based implementation in MATLAB. The simulations are carried out and the results are validated using the extracted circuit parameters from the manufacturer's data sheet under STC conditions. As the output voltage of PV is quite low, a boost converter is implemented to increase its voltage level. The boost converter is controlled by a MPPT algorithm namely, P & O to track the maximum power of the PV system. The stepped-up DC voltage is brought to a common DC bus bar to which DG2, i.e WECS of the MG is also connected. The resultant power rating of modeled PV generator is 3 kW with 14 numbers of panels, each has a power rating of 245W maximum. Similarly, the complete equation-based modeling of WECS including a wind turbine, PMSG, the boost converter is developed and simulated in MATLAB/Simulink. The DC voltage available at the common DC bus is converted to AC using voltage source converter to get a 3-phase distribution level voltage of 415V at the common AC bus. Further various linear and non-linear loads are delivered from this AC bus. The developed system along with its controllers has been investigated for the real-time data. The actual environmental data like solar irradiation and wind profile have been collected with the help of weather monitoring system of Birla Institute of Technology and Science, Hyderabad campus. The record of solar insolation and wind speed during different periods is observed. The output voltage and P responses in case of PV generating system due to the variation in solar irradiation, the output voltage and P, Q responses in case of WECS due to the change in wind speed are observed and presented. Due to

these frequent variations and also due to the nature of loads (harmonic and reactive) connected, power quality issues are observed concluding the requirement of reactive power compensation in the MG. Further, a custom power device acting as a power quality compensator in the proposed MG to mitigate all these issues is recommended.